Supplement of Atmos. Chem. Phys., 19, 13809–13825, 2019
https://doi.org/10.5194/acp-19-13809-2019-supplement

Supplement of

Analysis of temporal and spatial variability of atmospheric CO_2 concentration within Paris from the GreenLITE™ laser imaging experiment

Jinghui Lian et al.

Correspondence to: Jinghui Lian (jinghui.lian@lsce.ipsl.fr)

Supplement

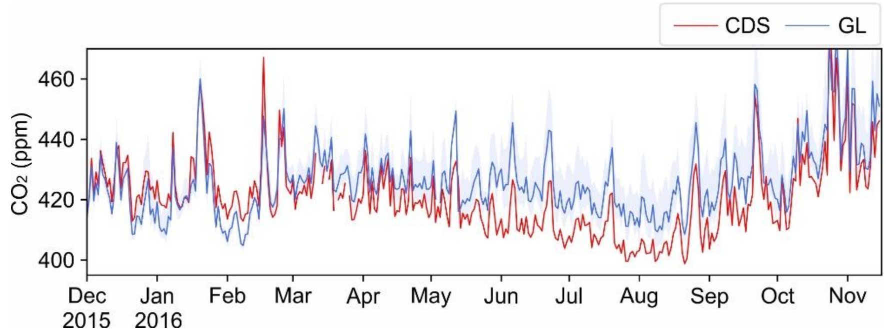

Figure S1: Daily average CO_2 concentrations between the original GreenLITE™ data and the CDS measurement. The shaded area indicates the 30 inter-chord range.

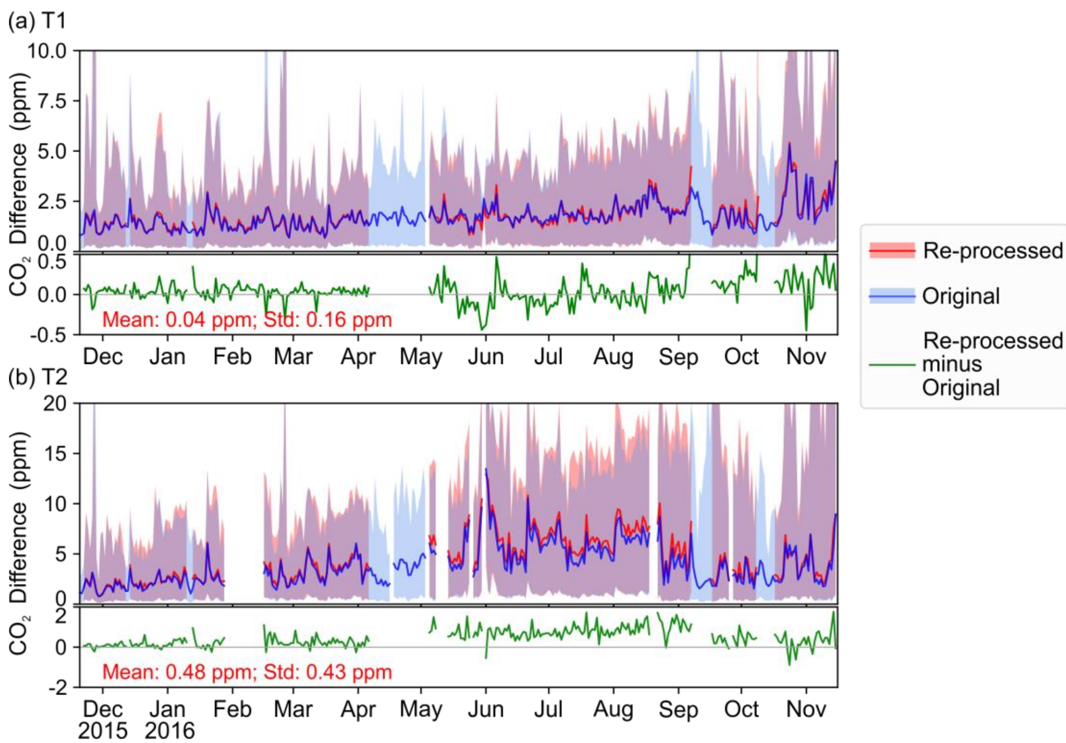

Figure S2: Distribution of the original and re-processed GreenLITE™ absolute CO_2 concentration differences between all pairs of chords for (a) T1 and (b) T2 from December 2015 to November 2016. The solid lines in top panels of (a) and (b) indicate the 0.5 quantile, and the shaded areas represent the 0.1 and 0.9 quantile intervals for original data in blue and re-processed data in red. The green line in bottom panels of (a) and (b) indicates the differences between the median values of the re-processed and original inter-chord range.

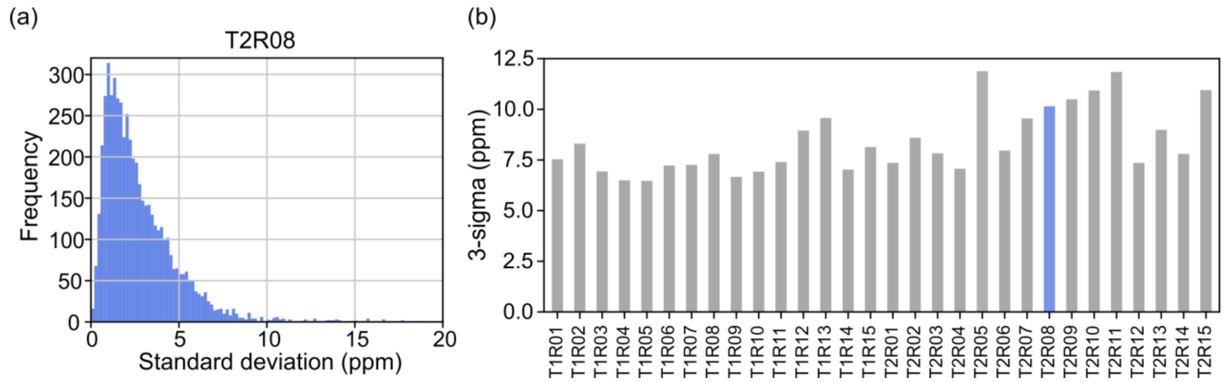

Figure S3: (a) Frequency distribution of the standard deviations of 4-minute CO_2 concentrations measured within one hour for one chord (e.g. T2R08); (b) Three-sigma threshold (mean + 3σ) of the standard deviations of the 4-minute measurements within a one-hour period for each chord.

The outlier detection for the 4-minute GreenLITE™ data is mainly based on the 3-sigma rule, which is used to remove the data outside three standard deviations from a mean in the positive direction. Figure S3 (a) shows the frequency distribution of the standard deviations of the 4-minute CO_2 concentrations measured within one hour for one given chord (e.g. T2R08). Figure S3 (b) shows the three-sigma threshold (mean + 3σ) of the standard deviations of the 4-minute measurements within a one-hour period for each chord. In general, the threshold varies between 6.5 ppm and 11.9 ppm from chord to chord. We therefore choose to use a uniform threshold value of 10 ppm to remove the outliers for all chords.

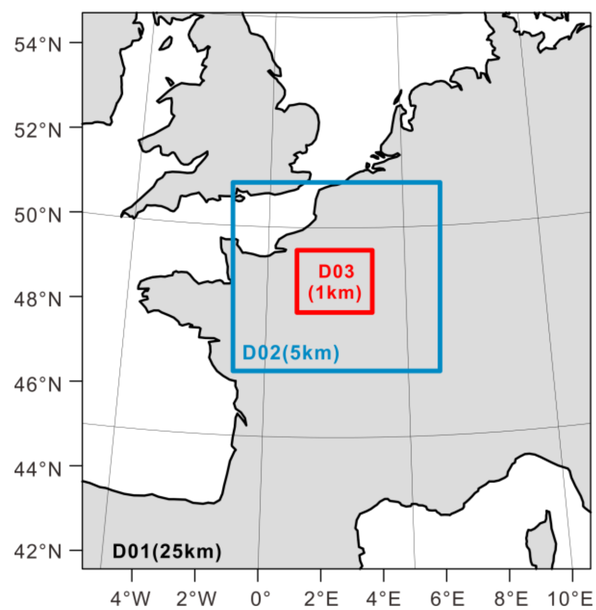

Figure S4: WRF-Chem domain settings.
(Data source: the continent-ocean boundary is from the NCAR Command Language (NCL) Ncarg4_1 database)

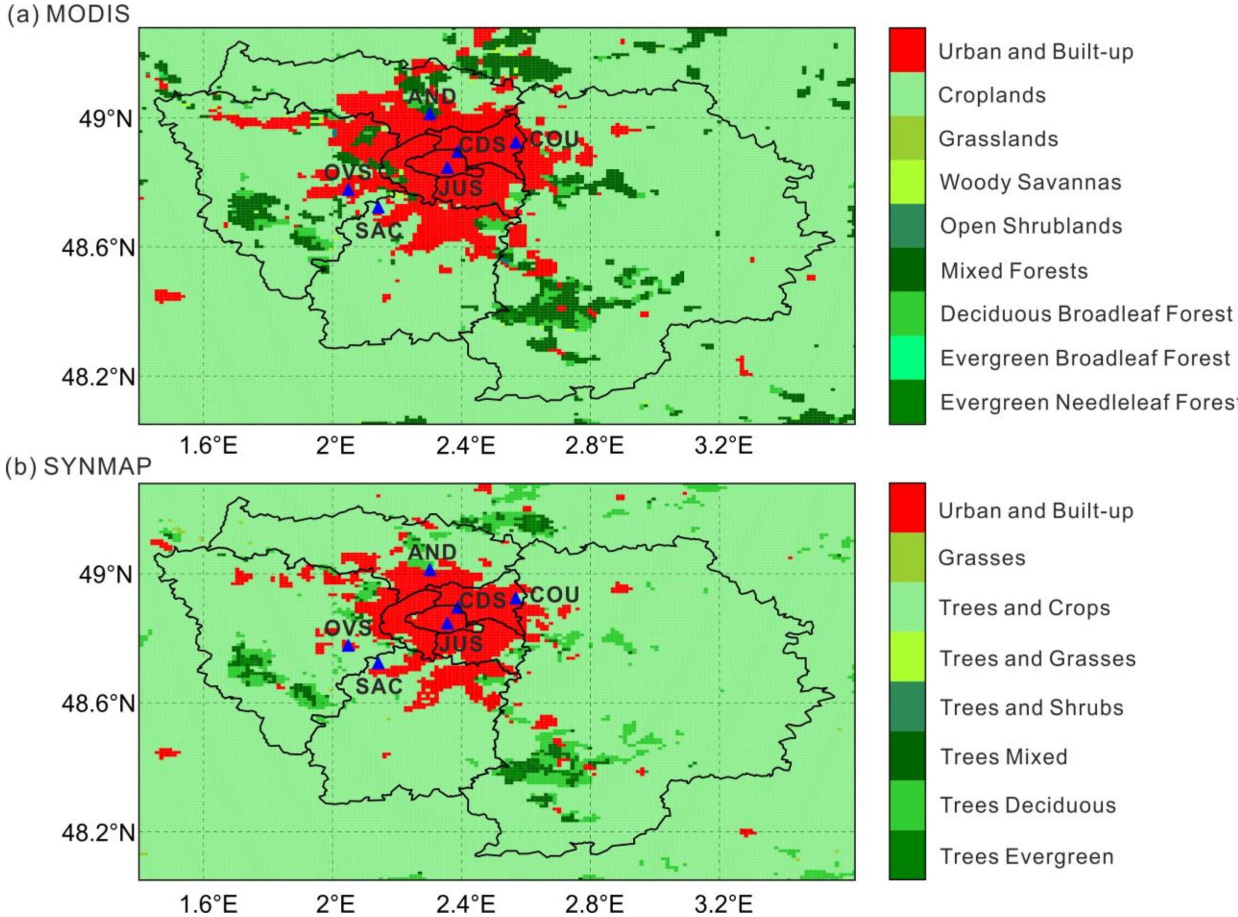

Figure S5: Dominant land use categories over the IdF region of Domain 03 from (a) MODIS database used in the WRF model and (b) SYNMAP database used in the VPRM model. Note that in the VPRM, it is the fractional vegetation coverage for a given grid cell covered by the respective land cover classes.

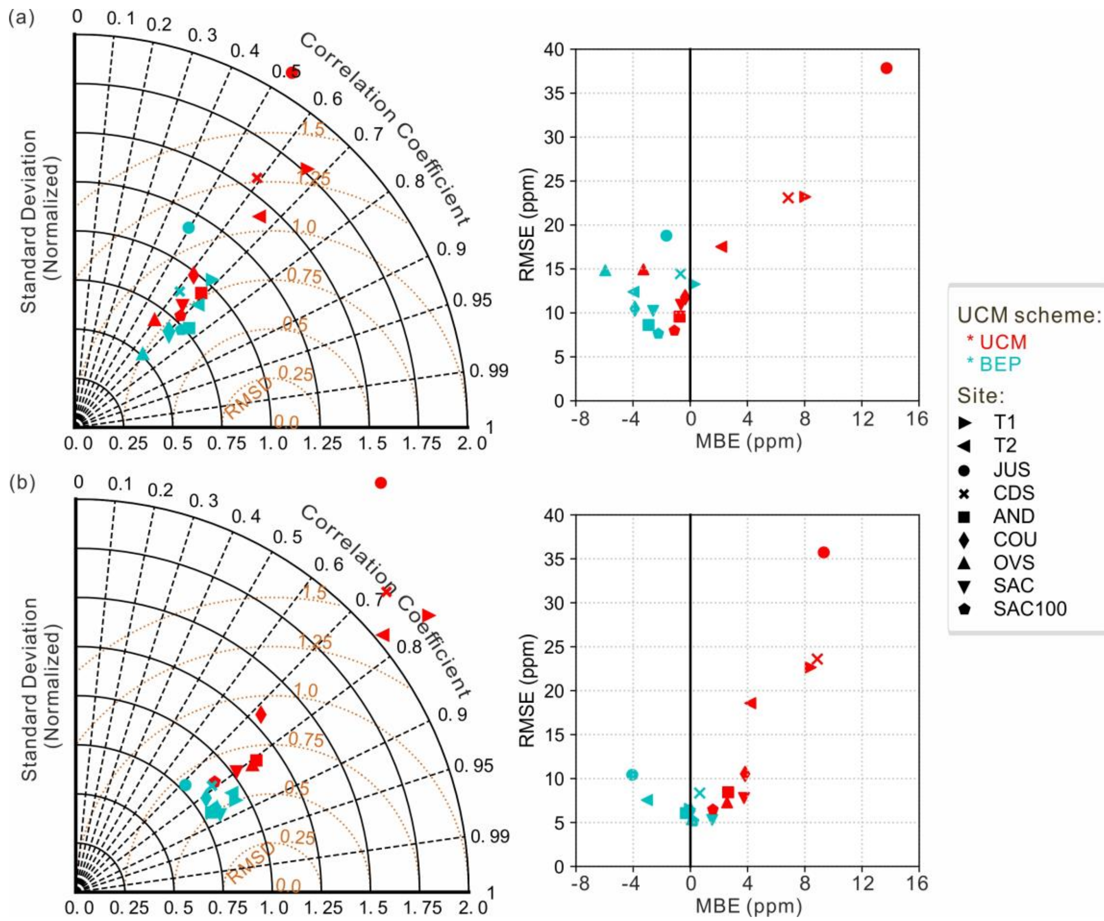

Figure S6: Normalized Taylor diagram (left) and RMSE versus MBE (right) for simulated (a) all hourly and (b) hourly afternoon (11-16 UTC) CO_2 concentrations from December 2015 to November 2016. The colors of markers indicate 2 different urban canopy schemes with UCM in red and BEP in cyan. In the Taylor diagram, normalized standard deviation is on the radial axis; Correlation coefficient is on the angular axis; Orange dashed lines indicate RMSD.

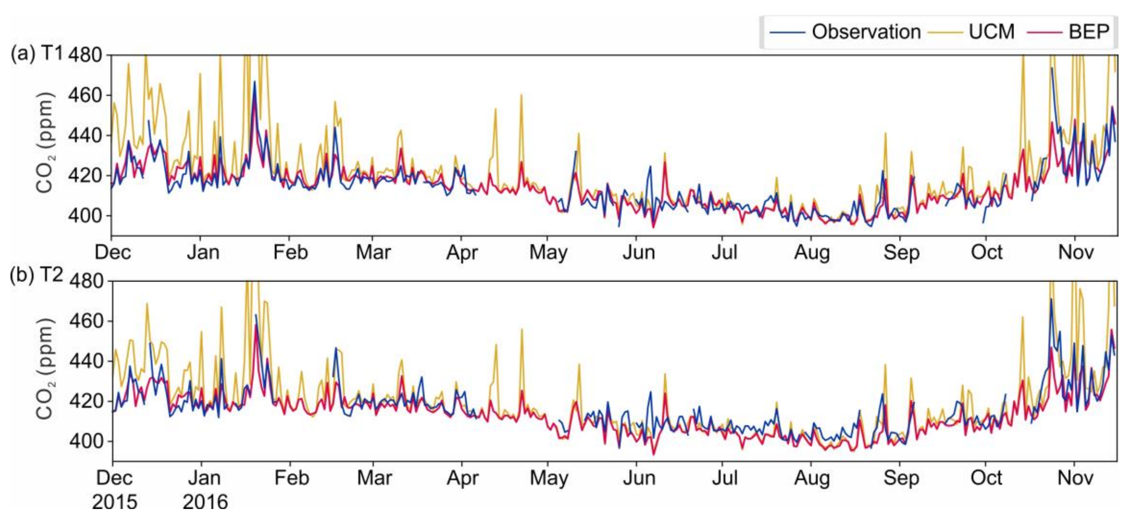

Figure S7: Time series of the GreenLITE™ observed and modeled averaged CO_2 concentrations during afternoon (11-16 UTC) for the (a) T1 and (b) T2 chord ensembles.

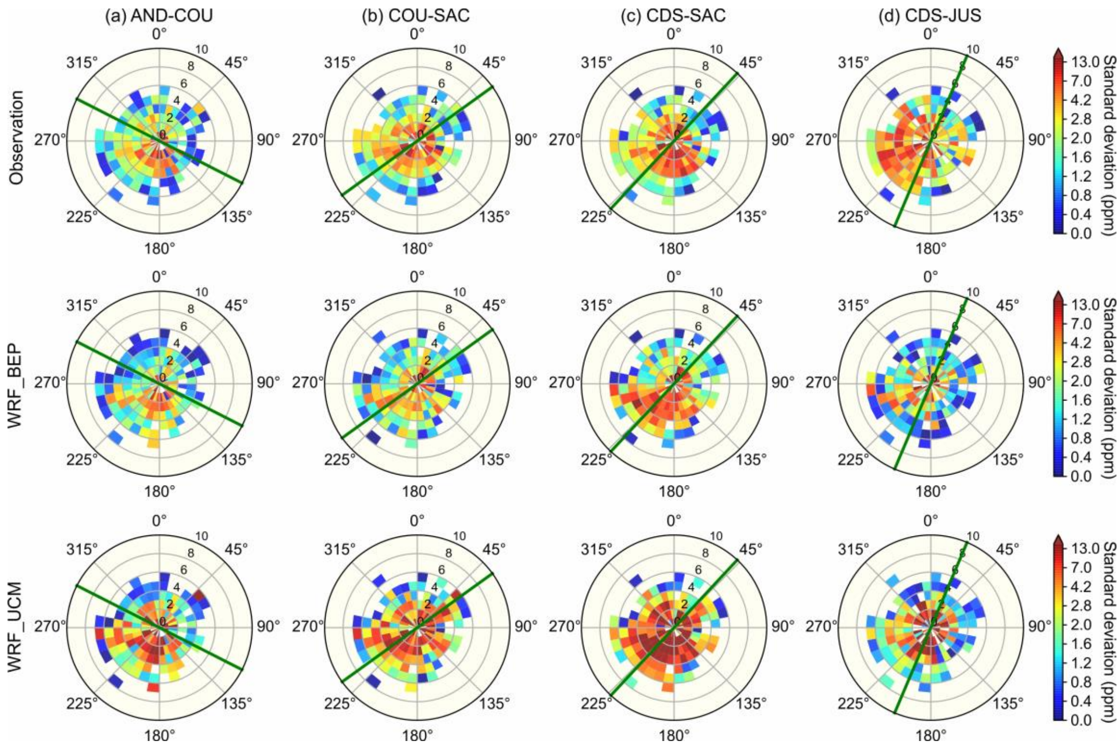

Figure S8: Standard deviations of spatial differences in CO_2 concentration between two stations of the in-situ network accounting for wind speed and direction. Only the afternoon (11-16UTC) data are used. The top row shows the observations, whereas the other two rows show the two simulations (UCM, BEP). The green line indicates the direction defined by two in-situ stations.

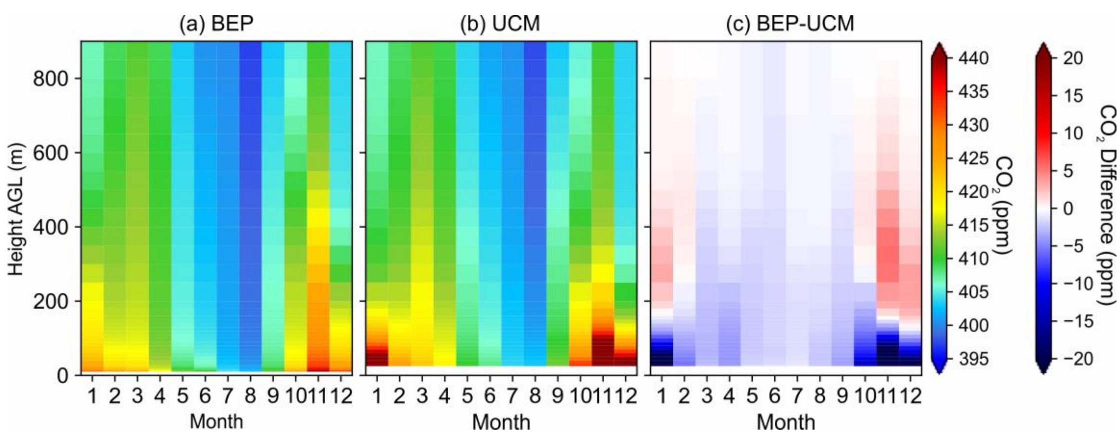

Figure S9: Vertical distributions of CO_2 concentrations during afternoon (11-16 UTC) at transceiver T2 (also JUS) for 12 calendar months for two simulations (a) BEP, (b) UCM, and (c) their differences.

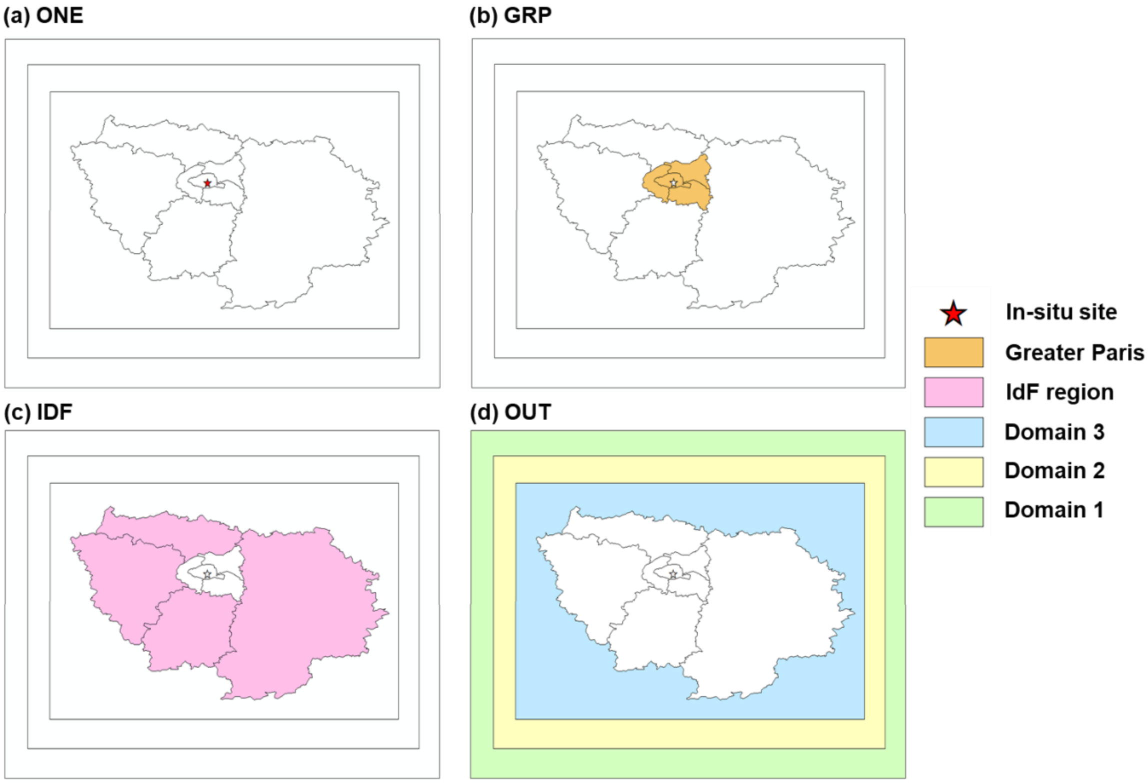

Figure S10. Four experiments are carried out for the JUS station with the assignment of emissions to: (a) ONE: one grid cell that contains an in-situ station; (b) GRP: all grid cells within the Greater Paris except the one where the station is located; (c) IDF: all grid cells within the IdF region except those of the Greater Paris; (d) OUT: all grid cells outside the IdF region. Another four experiments are carried out for the COU station.

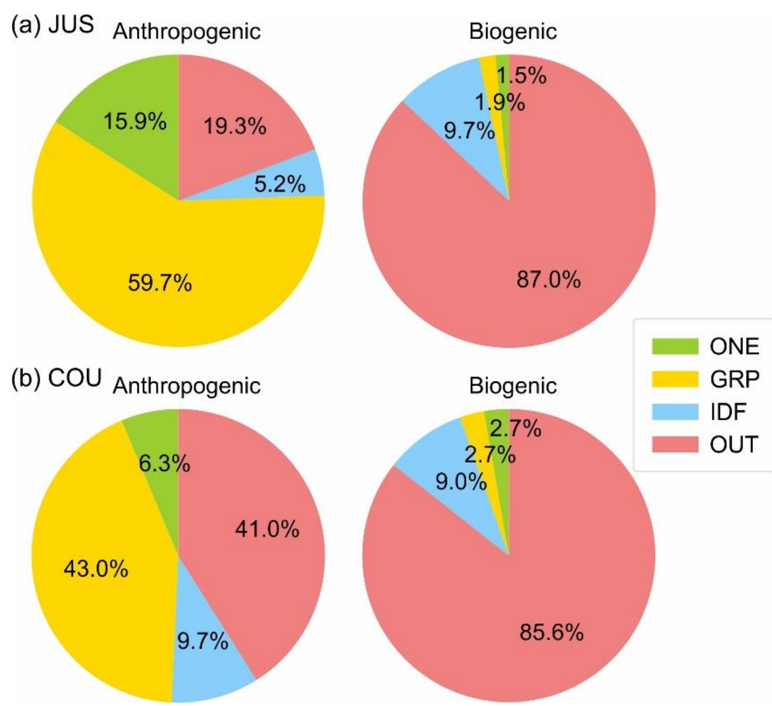

Figure S11. Relative contributions (in percentages) of each component flux to the modeled total anthropogenic and biogenic CO_2 concentrations for (a) urban site JUS and (b) suburban site COU. Note that only the afternoon data (11-16 UTC) are used in the analysis.

In order to determine respective contributions of various areas/sectors to the simulated CO_2 concentrations at a certain measurement site, we carried out a set of sensitivity experiments for the one-month period of March 2016 with anthropogenic and biogenic emissions limited to a given area within the simulation domain. This set of experiments includes the assignment of emissions to: 1) ONE: one grid cell that contains an in-situ station, 2) GRP: all grid cells within the GReater Paris except the one where the station is located, 3) IDF: all grid cells within the IdF region except those of the Greater Paris, 4) OUT: all grid cells outside the IdF region, as shown in Figure S10 (a) (b) (c) (d) respectively. The contribution from sources outside the model domain is small enough so that its influence is negligible. Figure S11 shows the relative contributions (in percentages) of each component to the modeled total anthropogenic and biogenic CO_2 concentrations for one urban site JUS and one suburban site COU respectively. The simulated monthly mean concentrations of anthropogenic CO_2 are 11.0 ppm at JUS and 5.4 ppm at COU, which are much larger than those of biogenic CO_2 (0.6 ppm at JUS and 0.7 ppm at COU). In general, an urban station like JUS is under a strong influence of the anthropogenic emissions within the IdF region. The contributions of anthropogenic emissions in the vicinity of the station (ONE) and from the Greater Paris (GRP) areas to the simulated anthropogenic CO_2 concentrations are around 16% and 60% respectively, whereas the remote anthropogenic emissions account for less than 20%. For a suburban station like COU, the Parisian emissions (GRP) and the remote ones (OUT) have a comparable influence (~40%) on the simulated anthropogenic concentrations, with very large variations depending on the wind direction (downwind or upwind of the city). Note that in these experiments, the emission inventory and the WRF-Chem modeling cannot describe the CO_2 patterns (both emission and concentration) at a scale finer than 1 km, and the simulation shows that the "local" contribution is significant. The unresolved spatial distribution of the emission can therefore be a significant contribution to the uncertainty. The biogenic CO_2 concentrations mainly come from outside of the IdF region (~86%).

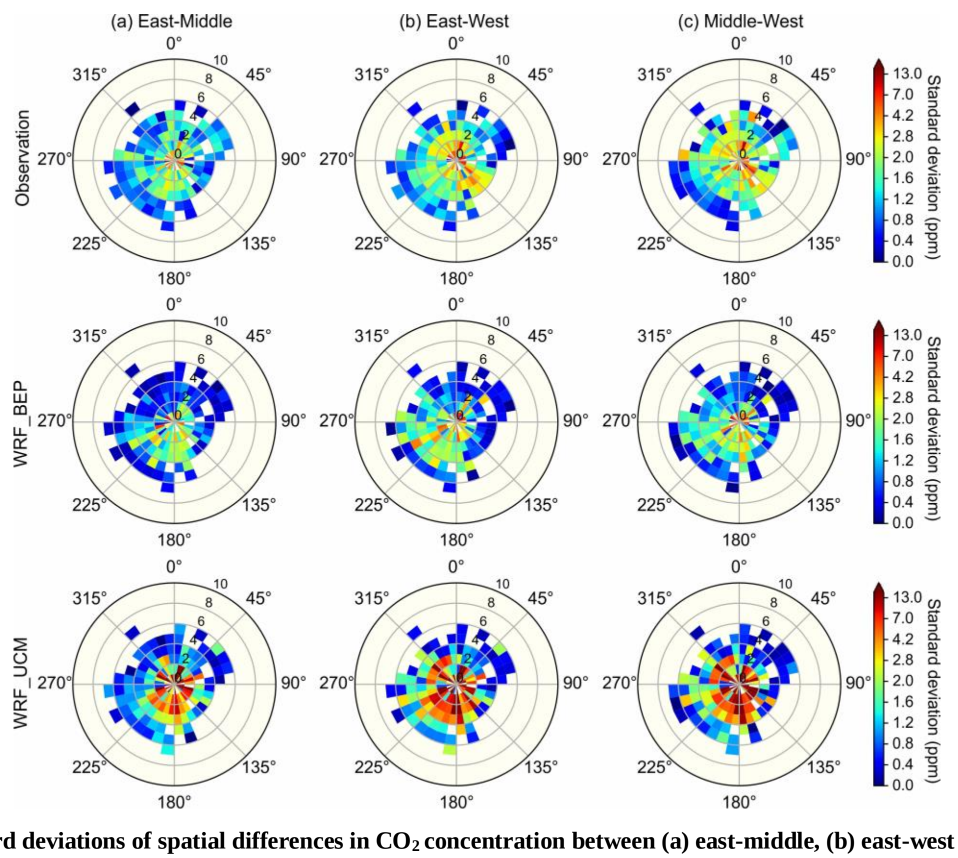

Figure S12: Standard deviations of spatial differences in CO_2 concentration between (a) east-middle, (b) east-west and (c) middle-west parts of the GreenLITE™ T1 measurement accounting for wind speed and direction. Only the afternoon (11-16UTC) data are used. The top row shows the observations, whereas the other two rows show the two simulations (UCM, BEP).

Table S1. National CO_2 emissions from fossil-fuel combustion and cement production for the countries within the WRF-Chem domain used in this study (unit: $MtCO_2$/yr). The data in the following table are taken from Le Quéré et al. (2018), available at https://www.icos-cp.eu/GCP/2018, last access: August 2019. (The use of data is conditional on citing the original data sources: data in black are from the CDIAC inventory (Boden et al., 2017), data in red are from the UNFCCC national inventory reports (UNFCCC, 2018), data in purple are from the BP Statistical Review of World Energy (BP, 2018). Cement emissions are updated from Andrews (2018))

	Austria	Belgium	France (including Monaco)	Germany	Italy (including San Marino)	Luxembourg	Netherlands	Spain	Switzerland	United Kingdom
2005	79.37	125.64	432.64	867.22	495.23	12.05	177.53	368.96	45.78	570.00
2010	72.38	113.58	397.90	833.68	424.87	11.15	182.18	283.88	45.05	512.21
2015	66.70	100.23	348.16	797.08	355.48	9.26	165.03	271.73	38.74	422.66
2016	67.40	100.24	350.10	801.75	350.32	9.00	165.52	260.99	39.20	398.55

Table S2. Seasonal statistics for observed and modeled all hourly CO_2 concentrations for two urban canopy schemes (UCM, BEP) from December 2015 to November 2016. DJF denotes December-January-February, MAM denotes March-April-May, JJA denotes June-July-August and SON denotes September-October-November. The color highlights the value in the cell with the minimum in blue, the median in white and the maximum in red. All other cells are colored proportionally.

(a) Correlation coefficient

		T1		T2		JUS 30m		CDS 34m		SAC 15m		SAC 100m	
		UCM	BEP	UCM	BEP	UCM	BEP	UCM	BEP	UCM	BEP	UCM	BEP
All hourly	DJF	0.68	0.67	0.58	0.67	0.62	0.63	0.49	0.51	0.68	0.77	0.59	0.73
	MAM	0.52	0.56	0.52	0.61	0.39	0.39	0.48	0.53	0.64	0.71	0.64	0.67
	JJA	0.63	0.61	0.60	0.60	NA	NA	0.52	0.55	0.68	0.72	0.59	0.63
	SON	0.55	0.58	0.57	0.63	0.47	0.46	0.55	0.54	0.57	0.65	0.64	0.70

(b) Root-mean-square error (RMSE. Unit: ppm)

		T1		T2		JUS 30m		CDS 34m		SAC 15m		SAC 100m	
		UCM	BEP	UCM	BEP	UCM	BEP	UCM	BEP	UCM	BEP	UCM	BEP
All hourly	DJF	28.26	11.23	19.38	11.03	40.96	14.43	28.84	13.63	8.82	7.42	7.47	6.64
	MAM	18.91	11.77	14.85	9.84	25.89	14.42	18.24	12.23	8.78	7.86	7.85	7.74
	JJA	9.98	10.33	10.13	10.09	NA	NA	12.11	11.00	11.48	11.49	7.14	7.20
	SON	32.94	20.06	25.23	18.11	43.50	24.22	29.57	20.27	13.82	13.20	9.46	8.97

(c) Mean bias error (MBE. Unit: ppm)

		T1		T2		JUS 30m		CDS 34m		SAC 15m		SAC 100m	
		UCM	BEP	UCM	BEP	UCM	BEP	UCM	BEP	UCM	BEP	UCM	BEP
All hourly	DJF	12.99	-0.36	6.75	-2.97	14.24	-3.85	12.09	-0.11	0.96	-0.89	-1.09	-1.62
	MAM	6.28	1.21	1.11	-3.32	8.65	-0.12	4.94	-0.62	0.03	-1.53	-1.30	-2.59
	JJA	1.25	0.97	-2.50	-3.68	NA	NA	1.77	0.74	-3.71	-4.38	-1.69	-2.72
	SON	14.06	-0.83	5.33	-6.20	17.70	-1.39	8.99	-3.05	-0.64	-3.98	-0.27	-2.01

References in the supplement:

Andrew, R. M.: Global CO_2 emissions from cement production, Earth System Science Data, 10, 195-217, https://doi.org/10.5194/essd-10-195-2018, 2018.

Boden, T. A., Marland, G., and Andres, R. J.: Global, Regional, and National Fossil-Fuel CO_2 Emissions, available at: http://cdiac.ornl.gov/trends/emis/overview_2014.html (last access: July 2017), Oak Ridge National Laboratory, U.S. Department of Energy, Oak Ridge, Tenn., USA, 2017.

BP: BP Statistical Review of World Energy June 2018, available at: https://www.bp.com/content/dam/bp/en/corporate/pdf/energy-economics/statistical-review/bp-stats-review-2018-full-report.pdf, last access: June 2018.

UNFCCC, 2018. National Inventory Submissions 2018. United Nations Framework Convention on Climate Change. Available at: http://unfccc.int/process/transparency-and-reporting/reporting-and-review-under-the-convention/greenhouse-gas-inventories-annex-i-parties/national-inventory-submissions-2018; accessed June 2018.